Small-Angle Oblique-Incidence Infrared Reflection in Polar Materials: II. Experiment on ZnO

Noritaka KURODA*[§], Yuji KUMAGAI[†], Takeshi HIMOTO[‡], and Hiroyuki YOKOI

Department of Materials Science and Engineering, Graduate School of Science and Technology, Kumamoto University, Kumamoto 860-8555, Japan

(Received December 14, 2009; accepted March 24, 2010; published , 2010)

The properties of polar optical phonons in thick single crystals of semi-insulating ZnO have been studied experimentally by infrared small-angle oblique-incidence reflectometry (SAOIR) with the subsidiary measurement of Raman scattering. The infrared light used is *s*- or *p*-polarized and incident to the *c*-face of the crystals at an angle of 10°. Despite such a small angle of incidence, since the principal components of the dielectric tensor are very small around the frequencies of longitudinal optical (LO) phonons, Snell's total reflection and Brewster's null reflection take place contiguously to modify the reststrahlen band. Consequently, a pair of line structures due to LO phonons of A_1 and E_1 modes appear in the difference spectrum between the *s* and *p* spectra. Analysis of the results in terms of Kuroda and Tabata's theory of SAOIR using the dielectric function of Gervais and Piriou's four-parameter semi-quantum oscillator model provides accurate frequencies and damping energies of all the LO and transverse optical (TO) phonons.

KEYWORDS: small-angle oblique-incidence reflection, infrared, Brewster's null reflection, Snell's total reflection, LO phonon, ZnO

---

*Present address: Free Laboratory for Materials Technology, Shimizunuma 2-10-18, Sendai 983-0845, Japan

[†]Present address: Fuji Electric Device Technology Co., Ltd., Matsumoto Branch, Matsumoto 390-0821, Japan

[‡]Present address: Ube Material Industries, Ltd., Ube 755-0043, Japan

[§]E-mail address: kurodaflmt@ac.auone-net.jp

1. Introduction

The reflection of light by a substance arises from the reemission of electromagnetic waves by electric dipoles induced in the substance by incident light. An electromagnetic wave emitted by an oscillating electric dipole has an axially symmetric profile of its power. One unique aspect of this radiation is that the flow of electromagnetic energy is absent on the line of the axis of the dipole. Consequently, upon oblique incidence of light from a medium to a planar interface against a different medium, if the light is polarized parallel to the plane of incidence and the sum of the angles of incidence and refraction is equal to $\pi/2$, no reflection of light occurs. This is known as Brewster's law[1]. In contrast, when the relative index of refraction of the interfacing medium is smaller than unity and the angle of incidence is greater than a critical value, the incident light is totally reflected. These Brewster's null reflection (hereafter referred to as BNR) and Snell's total reflection (hereafter referred to as STR) have been put to various practical uses in the optical engineering of materials.

Recently, Kuroda, one of the present authors, and Tabata[2] have theoretically studied the oblique-incidence reflection of *s*-polarized and *p*-polarized infrared lights due to polar optical phonons in insulating polar materials at small angles of incidence of typically 10°. The notations *s* and *p* signify the directions of the electric field of light that are perpendicular and parallel to the plane of incidence, respectively. Kuroda and Tabata have focused their attention on the fact that the principal components of the dielectric tensor in insulating polar materials have small values at frequencies around longitudinal optical (LO) phonons, that is, every principal component is negative below the frequency ω_{LO} of a certain LO phonon but increases monotonically with increasing frequency to become positive above ω_{LO}.[3] In this situation, in contrast to the case of normal-incidence reflection, BNR and STR take place contiguously, giving rise to steep minima and maxima in close vicinity to ω_{LO} in the reflection spectrum. This small-angle oblique-incidence reflectometry (SAOIR) is similar to infrared spectral ellipsometry[4], but is different from it in the sense that the angle of incidence is set to be so large as 55–75° in standard spectral ellipsometry. The most remarkable aspect of the spectrum obtained from SAOIR is the fact that the responses from LO phonons are observed as line structures. This SAOIR technique has been employed for characterizing film/substrate systems of GaN/sapphire[5, 6] and ZnO/sapphire [7]. In the present study, we apply this technique to thick single crystals for the first time.

Structurally anisotropic materials play major roles in current short-wavelength optical devices. Blue- and white-light-emitting diodes are composed of multiple quantum wells of GaN, InGaN, and AlGaN. These III-nitride semiconductors have a crystal structure of the hexagonal wurtzite type. ZnO is another wide-gap semiconductor having the wurtzite structure, and has attracted much attention since the violet electroluminescence of a *p*-*i*-*n* junction has been reported.[8)] Wide-gap semiconductors have an advantage in that they are transparent for infrared-visible radiation. Therefore, they are favorable for use as ultraviolet ozone sensors for monitoring environmental air pollution, as well as for use as flat electrodes for solar cells. [9)]

The development of new photonic devices requires accurate knowledge of the electronic and lattice properties of the constituent substances. As has been reported for GaN films,[5, 6, 10)] the properties of polar optical phonons reflect the lattice quality and residual stress of the films. The shift in the phonon frequencies from those of unstrained bulk crystals provides information on residual stress. The damping energies of polar optical phonons tell us about the lattice quality and even about the depth profile of the lattice quality of the films. In addition, the observation of the coupling of LO phonons with a plasmon of free carriers yields quantitative information on the free-carrier parameters without measurements of transport properties.[11, 12)]

The properties of phonons in bulk-crystalline ZnO, however, are not established yet, although vibrational properties have been studied extensively by infrared reflection[12, 13)] and Raman scattering measurements[11, 14–19)]. In those works, the transverse optical (TO) phonons have been observed at 378–380 cm^{-1} for $\boldsymbol{E}||\boldsymbol{c}$, but the data obtained for $\boldsymbol{E}\perp\boldsymbol{c}$ scatter in a region of 407–413 cm^{-1}, where $\boldsymbol{E}$ and $\boldsymbol{c}$ are the electric field of radiation and the *c*-axis of the crystal, respectively. The data on the frequencies of LO phonons scatter more widely in the regions of 570–579 cm^{-1} and 583–592 cm^{-1} for $\boldsymbol{E}||\boldsymbol{c}$ and $\boldsymbol{E}\perp\boldsymbol{c}$, respectively. One reason for the difficulty in accurately determining those phonon frequencies is the presence of large angular dispersions[14, 15)] of polar optical phonons, which is common to heterogeneous anisotropic compounds.

The purpose of the present study is to experimentally search for the intrinsic properties of polar optical phonons, particularly of LO phonons, in ZnO using SAOIR. In §2, we present the physical basis of STR and BNR in the infrared SAOIR spectrum of ZnO crystals. The

experimental procedure is described in §3, and the results of experiment for thick single crystals of nearly insulating ZnO are presented and discussed in §4.

2. Physical Basis of Infrared SAOIR for *c*-Face of ZnO

We deal with the oblique-incidence reflection of linearly polarized infrared light from the plane *c*-face of a ZnO crystal. The optical configuration of the experiment is shown in Fig. 1. Representing the angle of incidence of light and the angle of refraction as θ and φ, respectively, from Snell's law, we have

$$\varepsilon(\omega)\sin^2\varphi = \sin^2\theta\,, \tag{1}$$

where $\varepsilon(\omega)$ is the dielectric function of the crystal and ω is the frequency of the infrared light. For clarity of the physical picture, we assume that $\varepsilon(\omega)$ is a real function of ω throughout this section unless otherwise noted. When $\varepsilon(\omega)$ is negative, the crystal does not transmit light, so that incident light is totally reflected. Equation (1) tells us that if $\varepsilon(\omega)$ is positive, but is smaller than $\sin^2\theta$, incident light is still totally reflected. Here, we refer to the former case as internal total reflection (ITR) by contrast with STR in the latter case. The usual, partial reflection takes place in the frequency region where $\varepsilon(\omega) > \sin^2\theta$. Since the *c*-axis is the optic axis in uniaxial crystals, *s*-polarized and *p*-polarized refracted lights propagate in the crystal as ordinary and extraordinary rays, respectively, in the optical configuration of the present study. Representing the principal dielectric function for the *a*- and *c*-directions as $\varepsilon_\perp(\omega)$ and $\varepsilon_\parallel(\omega)$, respectively, the dielectric function $\varepsilon_s(\omega)$ for *s*-polarized light is given by

$$\varepsilon_s(\omega) = \varepsilon_\perp(\omega)\,, \tag{2}$$

whereas $\varepsilon_p(\omega)$ for *p*-polarized light is given by

$$\frac{1}{\varepsilon_p(\omega)} = \frac{\sin^2\varphi}{\varepsilon_\parallel(\omega)} + \frac{\cos^2\varphi}{\varepsilon_\perp(\omega)}\quad. \tag{3}$$

By applying eq. (1) to $\varepsilon_p(\omega)$, we may rewrite eq. (3) into

$$\varepsilon_p(\omega) = \varepsilon_\perp(\omega) + \sin^2\theta - \frac{\varepsilon_\perp(\omega)}{\varepsilon_\parallel(\omega)}\sin^2\theta\,. \tag{4}$$

Let us represent the phonon-polariton states that give $\varepsilon_\parallel(\omega) = \sin^2\theta$ and $\varepsilon_\perp(\omega) = \sin^2\theta$ as $S_\parallel$ and

$S_\perp$, respectively, and the LO phonons polarized $\|\boldsymbol{c}$ and $\perp\boldsymbol{c}$ as $LO_\|$ and $LO_\perp$, respectively. Then, remembering that $LO_\|$ gives $\varepsilon_\|(\omega) = 0$ and $LO_\perp$ gives $\varepsilon_\perp(\omega) = 0$ in insulating polar materials,[3] we find from eq. (2) that $S_\perp$ becomes the upper or lower bound of STR for *s*-polarization, whereas from eq. (4), we find that $S_\|$ or $LO_\perp$ becomes the upper or lower bound of STR for *p*-polarization.

The reflectivity R_s of *s*-polarized light and R_p of *p*-polarized light are known to be given by[2, 20, 21]

$$R_s = \left| \frac{\cos\theta - \sqrt{\varepsilon_\perp(\omega) - \sin^2\theta}}{\cos\theta + \sqrt{\varepsilon_\perp(\omega) - \sin^2\theta}} \right|^2 \tag{5a}$$

and

$$R_p = \left| \frac{\sqrt{\varepsilon_\|(\omega)\varepsilon_\perp(\omega)}\cos\theta - \sqrt{\varepsilon_\|(\omega) - \sin^2\theta}}{\sqrt{\varepsilon_\|(\omega)\varepsilon_\perp(\omega)}\cos\theta + \sqrt{\varepsilon_\|(\omega) - \sin^2\theta}} \right|^2 . \tag{5b}$$

It is evident from eqs. (5a) and (5b) that BNR occurs only in *p*-polarization. The frequency of BNR is one of the two solutions of

$$\varepsilon_\|(\omega)\varepsilon_\perp(\omega)\cos^2\theta = \varepsilon_\|(\omega) - \sin^2\theta . \tag{6}$$

Since we set $\sin^2\theta << 1$ in SAOIR, the frequency of BNR is the one closer to the frequency of $LO_\|$ of the two solutions. If we take $\varepsilon_\|(\omega) = \varepsilon_\perp(\omega) \equiv \varepsilon(\omega)$, eq. (6) gives the BNR equation of $\varepsilon(\omega) = \tan^2\theta$, in agreement with the formula in an isotropic substance [1]. The other solution gives the frequency of the lattice-plasma antiresonance. For *s*-polarized light, the lattice-plasma antiresonance takes place at ω satisfying $\varepsilon_\perp(\omega) = 1$.

Normal modes of lattice vibrations in ZnO, which has a wurtzite structure of a C_{6v} point symmetry, are represented as

$$\Gamma = 2A_1 + 2B_1 + 2E_1 + 2E_2 \ . \tag{7}$$

One A_1 and one E_1 modes are acoustic modes and the other A_1 and E_1 modes are infrared and Raman-active optical modes, whereas two E_2 modes are optical but only Raman-active and the two B_1 modes are both infrared and Raman-inactive. Consequently, there is one ITR band, being called reststrahlen band, for each of the polarizations $\boldsymbol{E}\|\boldsymbol{c}$ and $\boldsymbol{E}\perp\boldsymbol{c}$, that is, a band due to the optical A_1 mode for $\boldsymbol{E}\|\boldsymbol{c}$ and a band due to the optical E_1 mode for $\boldsymbol{E}\perp\boldsymbol{c}$. Practically, the

dielectric tensor responsible for this phonon system is a complex function of ω. Writing the frequency of the TO phonon as ω_{TO}, the dielectric tensor can be expressed in terms of the four-parameter semi-quantum oscillator model introduced by Gervais and Piriou as[22)]

$$\varepsilon_{\parallel,\perp}(\omega) = \varepsilon_{\infty\parallel,\perp} \frac{\omega^2 - \omega_{LO\parallel,\perp}^2 + i\gamma_{LO\parallel,\perp}\omega}{\omega^2 - \omega_{TO\parallel,\perp}^2 + i\gamma_{TO\parallel,\perp}\omega} \quad , \tag{8}$$

where ε_∞ is the optical dielectric constant, and $\gamma_{LO(TO)}$ is the damping energy of the LO(TO) phonon. Here, we deal with an ideal situation that TO and LO phonons undergo negligible damping, namely, $\gamma_{TO\parallel,\perp} = \gamma_{LO\parallel,\perp} = 0$. In this situation, it is evident from eq. (8) that for ω above $\omega_{TO\parallel,\perp}$, $\varepsilon_{\parallel,\perp}(\omega)$ is real and a monotonically increasing function of ω with a zero at $\omega_{LO\parallel,\perp}$. The small $\varepsilon_{\parallel,\perp}(\omega)$ at around $\omega_{LO\parallel,\perp}$ is crucial to STR and BNR in SAOIR.

Figure 2 shows the spectra calculated from eqs. (5a), (5b), and (8) with phonon frequencies $\omega_{TO(LO)\parallel}$ = 378.7(575.0) cm^{-1} and $\omega_{TO(LO)\perp}$ = 409.0(590.0) cm^{-1}, and the constants $\varepsilon_{\infty\parallel}$ = 3.78 and $\varepsilon_{\infty\perp}$ = 3.70 determined by Ashkenov *et al.*[13)] The phonon frequencies are derived experimentally in the present study: Details of the derivation are described in the next section. Concerning the anisotropy of the phonon structure, we have $\omega_{TO\parallel} < \omega_{TO\perp} < \omega_{LO\parallel} < \omega_{LO\perp}$, showing that ZnO belongs to the category of GaN-type crystals[2)]. The calculation is made with θ = 10° in accord with our experiment. Note that the reststrahlen band, which should spread flat from $TO_\perp$ to $LO_\perp$ in the normal-incidence reflection, is modified significantly in the region of LO phonons. Also noteworthy are the frequencies of the polariton states $S_\parallel$ and $S_\perp$. They can be obtained from combining eq. (8) with the aforementioned definitions of $S_\parallel$ and $S_\perp$ as

$$\omega_{S\parallel,\perp}^2 = \omega_{LO\parallel,\perp}^2 + \frac{(\omega_{LO\parallel,\perp}^2 - \omega_{TO\parallel,\perp}^2)\sin^2\theta}{\varepsilon_{\infty\parallel,\perp} - \sin^2\theta} \quad . \tag{9}$$

We confirm from Fig. 2 that $S_\parallel$ and $S_\perp$ serve as reflection edges of the SAOIR spectrum.

Interestingly, despite the fact that the total reflection is seen at frequencies from $TO_\perp$ up to $S_\perp$(591.3 cm^{-1}) in *s*-polarization, the total reflection breaks down halfway in a narrow region between $LO_\parallel$(575.0 cm^{-1}) and $S_\parallel$(576.3 cm^{-1}) in *p*-polarization. This breakdown is caused by the fact that, even though $\varepsilon_\perp(\omega)$ is negative, the collapse of the screening of the *c*-component of $\boldsymbol{E}$ by lattice vibrations of the A_1 mode makes $\varepsilon_p(\omega)$ positive and greater than $\sin^2\theta$ at frequencies between $LO_\parallel$ and $S_\parallel$. In this case, $S_\parallel$ is the lower-frequency bound of the

STR of which the upper bound connects to a band of ITR. This ITR is terminated by a narrow STR region of which the upper bound is $LO_{\perp}$. The condition for Brewster's angle given by eq. (6) holds just below $S_{\parallel}$, and thereby BNR occurs at 576.0 cm^{-1} in *p*-polarization as indicated by B in Fig. 2.

3. Experimental Procedure

Commercial synthetic crystals of ZnO (CrysTec) are used as the samples. The crystals are grown by a hydrothermal method without intentional doping so that the Hall concentration of electrons is of the order of 10^{12} cm^{-3} and the Hall mobility is ~120 $cm^2/(Vs)$. They are ~0.6-mm-thick plates with plane surfaces normal to the *c*-axis, one of which is Zn-polar and the other is O-polar. We measure the infrared SAOIR spectrum from both faces and conduct a subsidiary measurement of Raman scattering from the side faces of these crystals.

The SAOIR spectrum is measured using FT/IR spectrometers (JASCO FT/IR-410, JASCO FARIS-1) with a spectral resolution of 1 cm^{-1}. By using the equipment for reflectometry (JASCO RF-81S), the infrared beam coming out of the interferometer of FT/IR-410 or FARIS-1 is folded and focused on the sample crystal at an angle of incidence of 10°. A rotating wire-grid polarizer is placed in front of RF-81S, and the infrared beam is polarized linearly to be normal (*s*-polarization) or parallel (*p*-polarization) to the plane of incidence. The degree of polarization is greater than 90% throughout the wavelength region examined. The measurement of Raman scattering is made with a triple-stage spectrograph (Spex 1877A) equipped with a CCD detector (ANDOR DV401-FI). The 514.5 nm line of an Ar-ion laser is used as the light source. All the experiments are performed at room temperature.

4. Experimental Results and Discussion

Figure 3 shows the results of SAOIR measurement for the Zn-polar *c*-face of ZnO crystals. Although being significantly broadened and suppressed by damping, a dip due to BNR at the $LO_{\parallel}$ edge of the A_1 mode is clearly observed on the shoulder of the reststrahlen band of *p*-polarization. Figure 4 shows a close-up of the region around the shoulder of the *s* and *p* spectra. In addition to the prominent feature due to BNR, the difference between the *s* and *p* spectra due to STR arising in the frequency region from $LO_{\perp}$ over $S_{\perp}$ is distinct on the higher-frequency side of BNR. The modification due to these BNR and STR becomes more

evident if we draw the spectrum of $R_p - R_s$, as shown in Fig. 5. The results for the O-polar face are identical to the results for the Zn-polar face within experimental errors.

As is evident from Fig. 2, the $A_1(TO_{\|})$ mode is almost silent in SAOIR in the optical configuration of this experiment. Hence, we measure Raman scattering from one side face of our sample crystal, for the scattering by this mode is known to be comparatively intense for the configurations $x(yy)x'$ and $x(zz)x'$.[13] The spectrum obtained for $x(yy)x'$ is shown in Fig. 6. There appear first-order scatterings due to the $A_1(TO_{\|})$ mode, the $E_1(TO_{\perp})$ mode, a nonpolar E_2 mode, and the $E_1(LO_{\perp})$ mode; moreover, several second or higher-order scatterings due to off-Γ phonons[13, 17] are observed. We may identify the $A_1(TO_{\|})$ mode at 378.7 cm^{-1}.

To interpret the observed bands of SAOIR quantitatively, we calculate the spectra of R_s and R_p from eqs. (5a) and (5b) by introducing nonvanishing damping energies γ's of TO and LO phonons into the dielectric function given by eq. (8). Note here that the infrared beam is focused by concave mirrors; therefore, the angle of incidence θ might have a significant breadth. Since the features of BNR and STR grow up nonlinearly with increasing θ,[2] the breadth of θ would strengthen such features. At the same time, as suggested by the arguments presented in §2, they would shift to some extent towards higher frequencies. Taking these properties into account, in the present study, we regard θ as the effective angle of incidence of our apparatus. Then, by choosing $\theta = 11.0°$ and adjusting the frequencies and damping energies of the respective phonon modes, we can reproduce the experimental spectra very well with the calculated spectra: The best-fit curves are shown in Figs. 3–5 along with experimental data. The effective value of θ is almost uniquely obtained from the observed intensities of the BNR and STR features, as shown in Fig. 5.

To see how the reststrahlen band is modified due to BNR and STR, we calculate the normal-incidence reflectivity $R_{\perp}$ taking $\theta = 0°$ without changing other quantities. The calculated curve of $R_{\perp}$ is compared with the observed and calculated *s* and *p* spectra in Fig. 4. The spectra of $R_p - R_{\perp}$ and $R_{\perp} - R_s$ are also shown in Fig. 5, demonstrating the contributions of BNR and STR clearly. As mentioned in the preceding paragraph, the minimum positions of the spectra of $R_p - R_{\perp}$ and $R_{\perp} - R_s$ deviate slightly from frequencies of $LO_{\|}$ and $LO_{\perp}$, respectively. Equation (9) suggests that the deviation increases in a manner of a quadratic function of θ for $\theta << 1$. In ZnO, if θ exceeds 5°, the deviation becomes larger than 0.1 cm^{-1}, reaching 0.7 and 0.4 cm^{-1} for BNR of $R_p - R_{\perp}$ and STR of $R_{\perp} - R_s$, respectively, at an

effective θ of 11.0° of our apparatus.

From the treatment described above, the frequencies and damping energies of all the modes except $TO_{\|}$, which has been observed by Raman scattering, can be obtained with accuracies of ±0.3 and ±0.5 cm^{-1}, respectively. The results are listed in Table I, and compared with the previously reported data. Our data are all found within the scattering ranges of the previous data.

5. Conclusions

We have studied the physical basis of STR and BNR due to optical phonons in the SAOIR spectrum from the *c*-face of ZnO crystals. We have measured *s*- and *p*-polarized SAOIR spectra in nearly insulating single crystals of ZnO by setting the angle of incidence θ at 10°. Raman scattering has also been measured to obtain the frequency of the $A_1(TO_{\|})$ phonon, which is almost silent in the present configuration of SAOIR. Employing the dielectric function of Gervais and Piriou's four-parameter semi-quantum oscillator model, and taking the effect of the instrumental breadth of θ into account, the observed STR and BNR features have been described in terms of Kuroda and Tabata's theory very well. Hence, accurate frequencies and damping energies of TO and LO phonons have been obtained.

It has long been conceived that, for a bulk crystal of polar materials including compound semiconductors, it is difficult to observe the first-order excitation of optical phonons as single-line structures by infrared spectroscopy. In SAOIR, however, STR and BNR may manifest themselves as a set of line structures due to LO phonons in the difference spectrum between *s*- and *p*-polarizations. This new technique has been successfully applied to ZnO in this study.

Acknowledgements

One of the authors (N. K.) is grateful to Dr. H. Tampo for providing him with valuable information on ZnO crystals. Another author (Y. K.) and N. K. are indebted to IR & Raman Applications Laboratory of JASCO Corporation for their technical support in performing the FT/IR experiment.

1) M. Born and E. Wolf: *Principles of Optics* (Pergamon Press, New York, 1974) 5th ed., Chap.1.5.
2) N. Kuroda and Y. Tabata: J. Phys. Soc. Jpn. **79** (2010) 024710.
3) C. Kittel: *Introduction to Solid State Physics* (John Wiley & Sons, New York, 1966) 3rd ed., Chap. 5.
4) M. Schubert, T. E. Tiwald, and C. M. Herzinger: Phys. Rev. B **61** (2000) 8187.
5) N. Kuroda, K. Saiki, Hasanudin, J. Watanabe, and M.-G. Cho: AIP Conf. Proc. **772**, *27th Int. Conf. Physics of Semiconductors* (*ICPS-27*), ed. J. Menéndez and C. G. Van de Walle (Melville, New York, 2005) p. 281.
6) N. Kuroda, T. Kitayama, Y. Nishi, K. Saiki, H. Yokoi, J. Watanabe, M-W. Cho, T. Egawa, and H. Ishikawa: Jpn. J. Appl. Phys. **45** (2006) 646.
7) Y. Kumagai, T. Himoto, H. Tampo, H. Yokoi, H. Shibata, S. Niki, and N. Kuroda: AIP Conf. Proc. **893**, *28th Int. Conf. Physics of Semiconductors* (*ICPS-28*), ed. W. Jantsch and F. Schäffler (Melville, New York, 2007) p. 317.
8) A. Tsukazaki, A. Ohtomo, T. Onuma, M. Ohtani, T. Makino, M. Sumiya, K. Ohtani, S. F. Chichibu, S. Fuke, Y. Segawa, H. Ohno, H. Koinuma, and M. Kawasaki: Nat. Mater. **4** (2005) 42.
9) S. J. Pearton, J. C. Zolper, R. J. Shul, and F. Ren: J. Appl. Phys. **86** (1999) 1.
10) D. G. Zhao, S. J. Xu, M. H. Xie, S. Y. Tong, and H. Yang: Appl. Phys. Lett. **83** (2003) 677.
11) B. H. Bairamov, A. Heinrich, G. Irmer, V. V. Toporov, and E. Zeigler: Phys. Stat. Sol. B **119** (1983) 227.
12) E. F. Venger, A. V. Melnichuk, L. Yu. Melnichuk, and Yu. A. Pasechnik: Phys. Stat. Sol. B **188** (1995) 823.
13) N. Ashkenov, B. N. Mbenkum, C. Bundesmann, V. Riede, M. Lorenz, D. Spemann, E. M. Kaidashev, A. Kasic, M. Schubert, M. Grundmann, G. Wagner, H. Neumann, V. Darakchieva, H. Arwin, and B. Monemar: J. Appl. Phys. **93** (2003) 126.
14) T. C. Damen, S. P. S. Porto, and B. Tell: Phys. Rev. **142** (1966) 570.
15) C. A. Arguello, D. L. Rousseau, and S. P. S. Porto: Phys. Rev. **181** (1969) 1351.
16) R. H. Callender, S. S. Sussman, M. Selders, and R. K. Chang: Phys. Rev. B **7** (1973) 3788.
17) J. M. Calleja and M. Cardona: Phys. Rev. B **16** (1977) 3753.

18) M. Tzolov, N. Tzenov, D. Dimova-Malinovska, M. Kailatzova, C. Pizzuto, G. Vitali, G. Zollo, and I. Ivanov: Thin Solid Films **379** (2000) 28; **396** (2001) 274.
19) H. Harima: J. Phys.: Condens. Matter **16** (2004) S5653.
20) L. P. Mosteller, Jr. and F. Wooten: J. Opt. Soc. Am. **58** (1968) 511.
21) P. Brüesch: *Phonons*: *Theory and Experiments II* (Springer-Verlag, Berlin, 1986) Appendix B.4.
22) F. Gervais and B. Piriou: J. Phys. C: Solid State Phys. **7** (1974) 2374.

Fig. 1 Optical configuration for the measurement of oblique-incidence reflection from *c*-face of a thick crystal of ZnO. $\boldsymbol{E}_s$ and $\boldsymbol{E}_p$ denote *s*- and *p*-polarized electric fields of light, respectively.

Fig. 2 Calculated spectra of SAOIR due to polar optical phonons from the *c*-face of ZnO crystal for *s*-polarization (dash-dotted line) and *p*-polarization (solid line) at $\theta = 10°$. In the calculation, phonons are assumed to undergo no damping.

Fig. 3 Experimental SAOIR spectra of the *c*-face of ZnO crystal for *s*-polarization (open circles) and *p*-polarization (solid circles) at $\theta = 10°$. Dotted and solid lines are the calculated spectra for *s*- and *p*-polarizations, respectively. The calculation is made for $\theta = 11.0°$. See text.

Fig. 4 Close-up of the portion of the shoulder on the higher-frequency side of the reststrahlen band of Fig. 2. The additional dash-dotted line is the calculated spectrum of the normal-incidence reflectivity.

Fig. 5 Experimental (solid circles) and calculated (solid line) spectra of $R_p - R_s$. Dotted and dash-dotted lines are the calculated spectra of $R_p - R_\perp$ and $R_\perp - R_s$, respectively.

Fig. 6 Raman scattering spectrum of ZnO for the configuration x(yy)x'. The features denoted as M are due to multiphonon scattering.

Table I. Frequencies (cm^{-1}) of polar optical modes in bulk crystalline ZnO. Numbers in parentheses are the damping energies (cm^{-1}).

Mode	Present work	Bairamov et al.[11]	Venger et al.[12]	Ashkenov et al.[13]	Damen et al.[14]	Arguello et al.[15]
$A_1(TO_{\parallel})$	*378.7±1.0(11±1)	378 (10)	380	379	380	380
$A_1(LO_{\parallel})$	575.0±0.2(9.5±0.2)	576 (12)	570	574.5	574	579
$E_1(TO_{\perp})$	409.0±0.3(13±0.5)	409.5 (12)	412	408.2	407	413
$E_1(LO_{\perp})$	590.0±0.3(11.5±0.5)	588 (9)	591	592.1	583	591

*From Raman scattering.

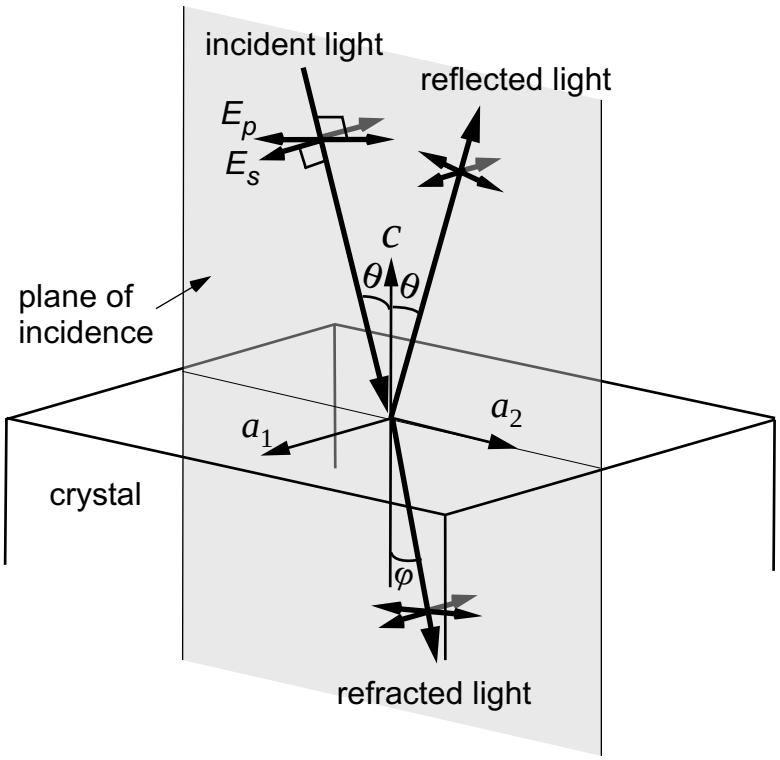
incident light
reflected light
E_p
E_s
c
θ
θ
plane of
incidence
a_1
a_2
crystal
φ
refracted light

Fig. 1

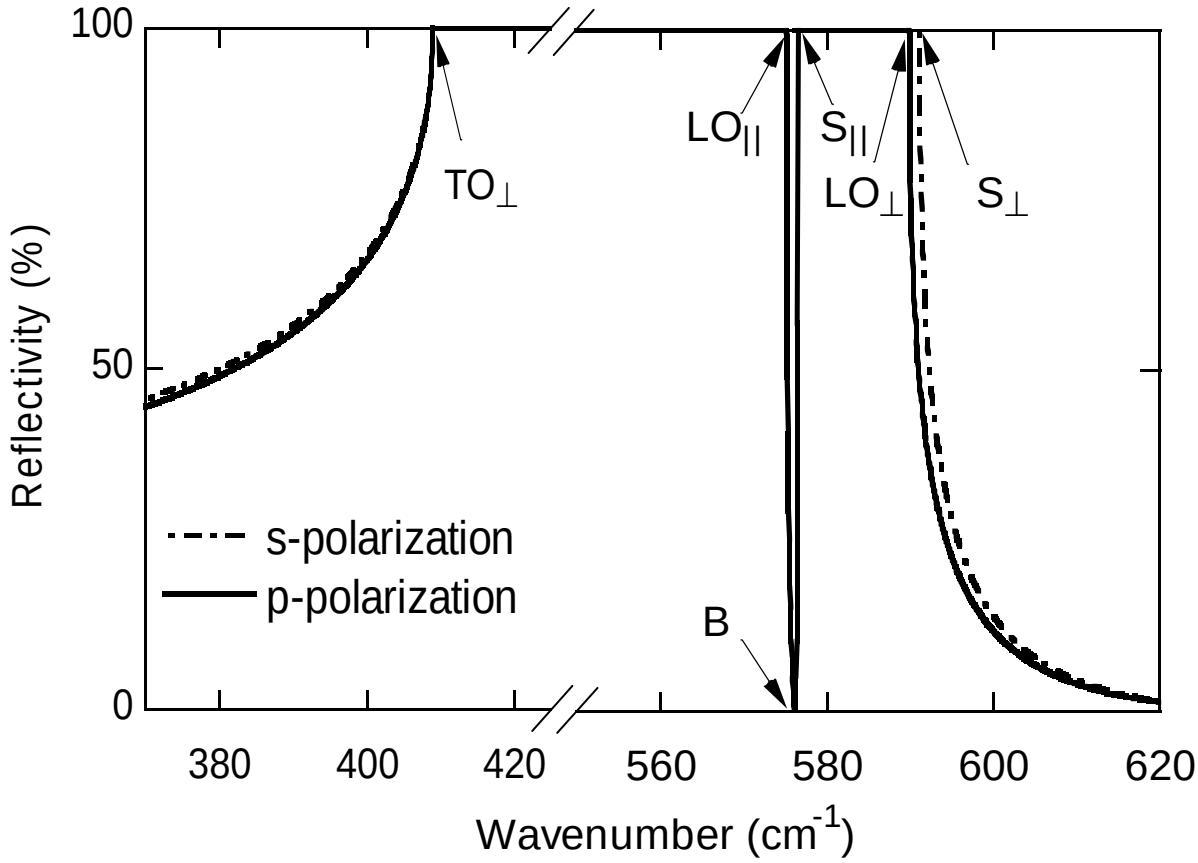
100
50
0
Reflectivity (%)
TO⊥
LO||
S||
LO⊥
S⊥
B
s-polarization
p-polarization
380
400
420
560
580
600
620
Wavenumber (cm-1)

Fig. 2

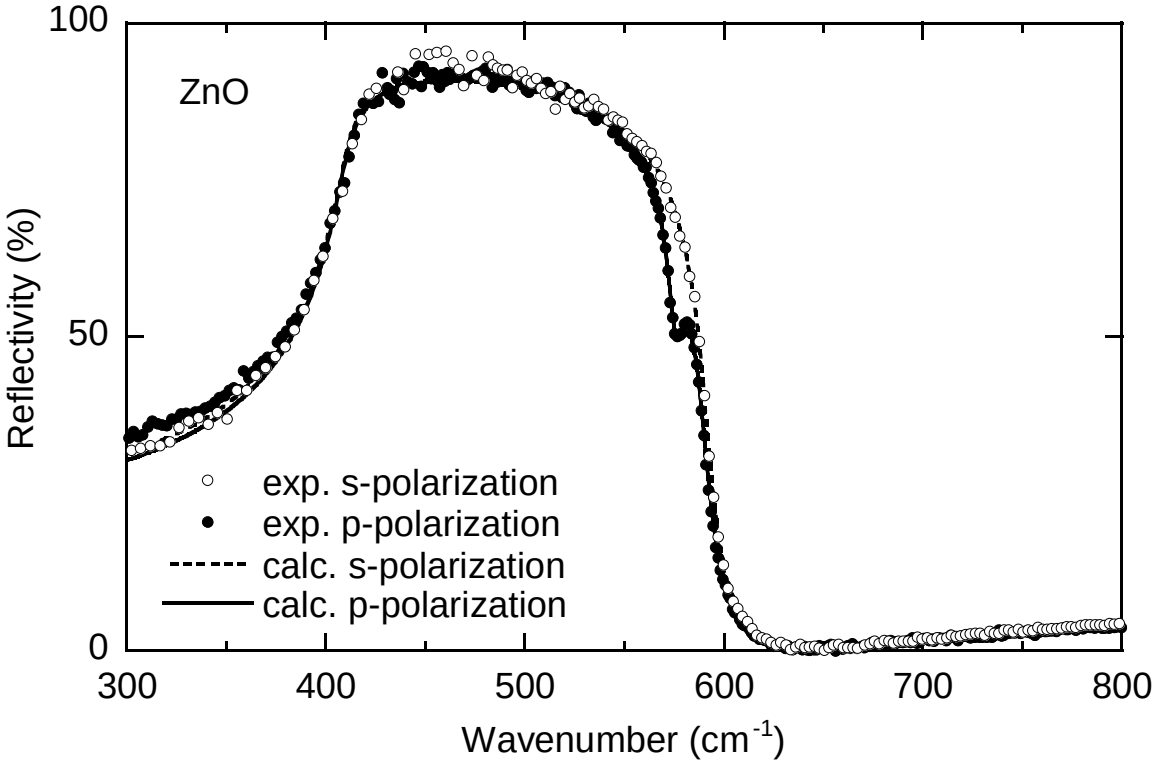
100
50
0
ZnO
Reflectivity (%)
exp. s-polarization
exp. p-polarization
calc. s-polarization
calc. p-polarization
300
400
500
600
700
800
Wavenumber (cm-1)

Fig. 3

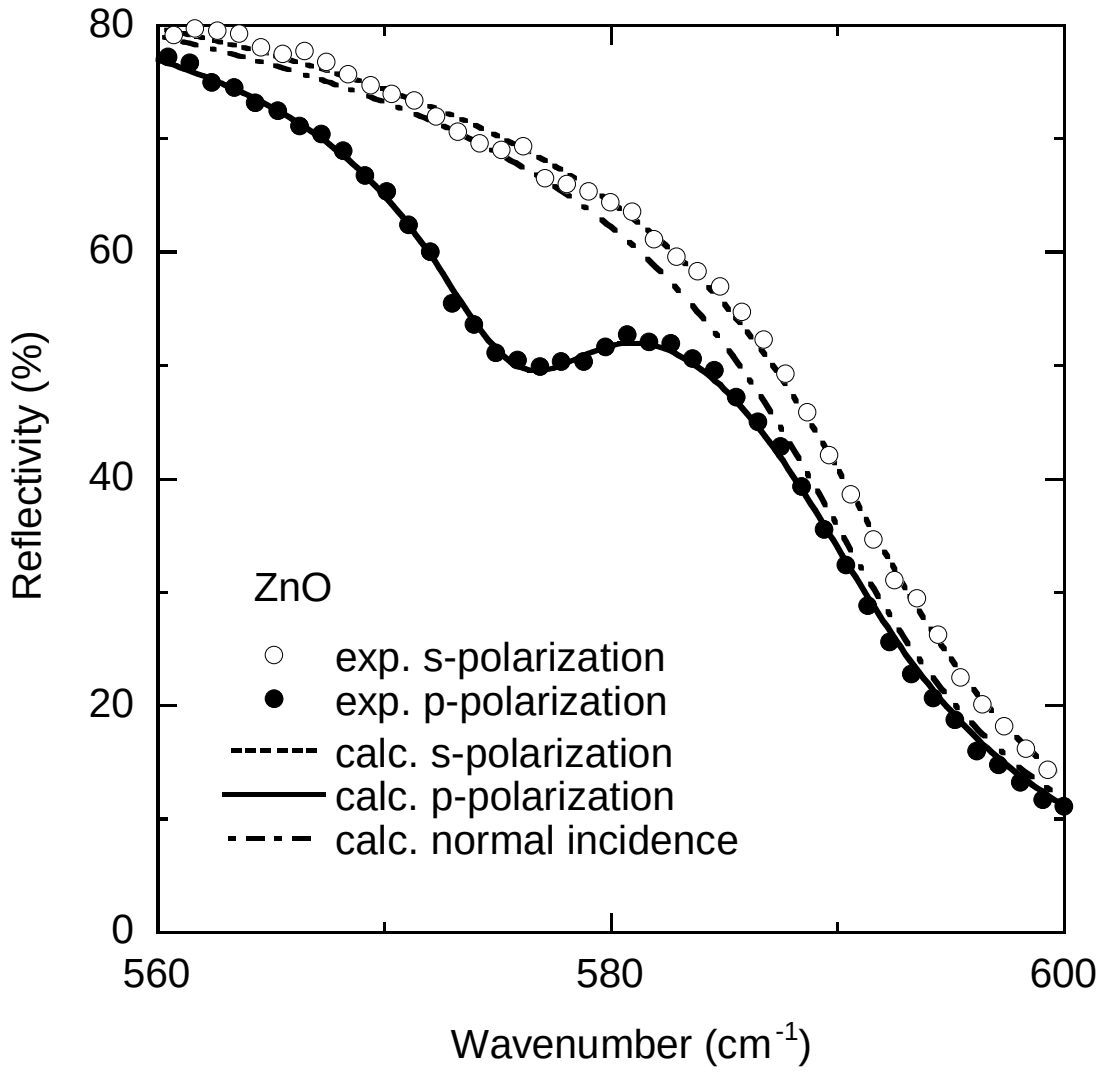
80
60
40
20
0
560
580
600
Reflectivity (%)
Wavenumber (cm-1)
ZnO
exp. s-polarization
exp. p-polarization
calc. s-polarization
calc. p-polarization
calc. normal incidence

Fig. 4

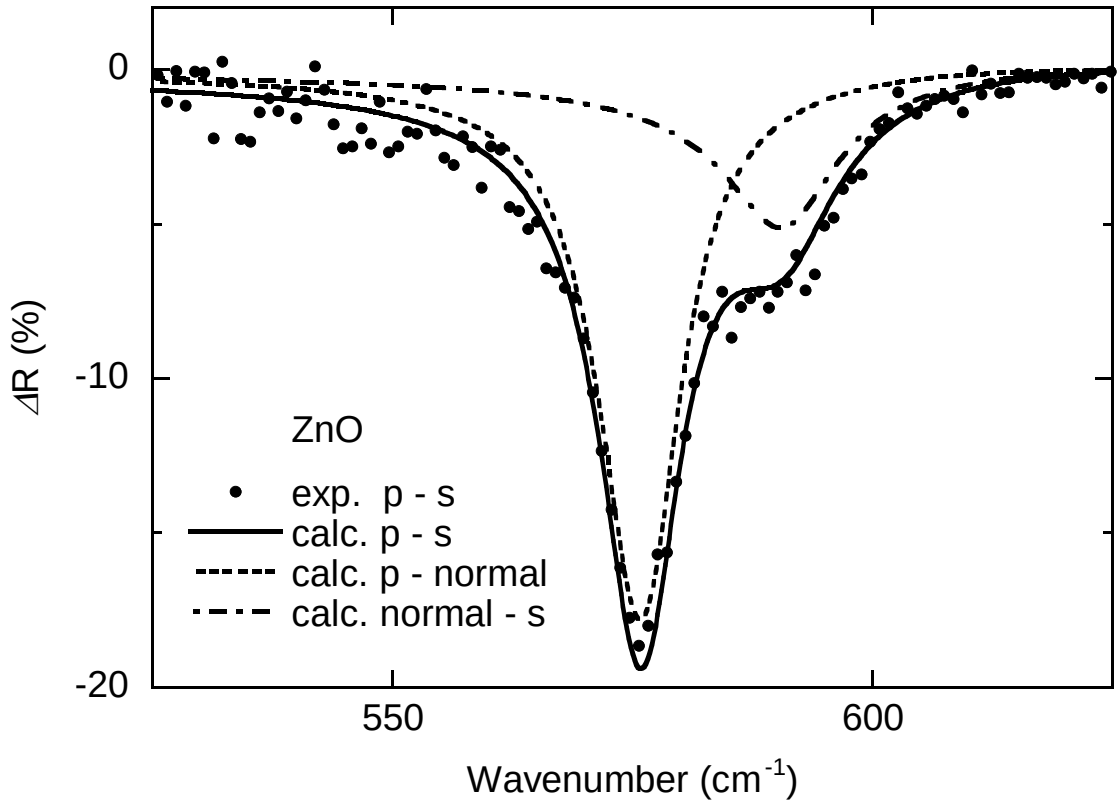
0
-10
-20
ΔR (%)
550
600
Wavenumber (cm-1)
ZnO
exp. p - s
calc. p - s
calc. p - normal
calc. normal - s

Fig. 5

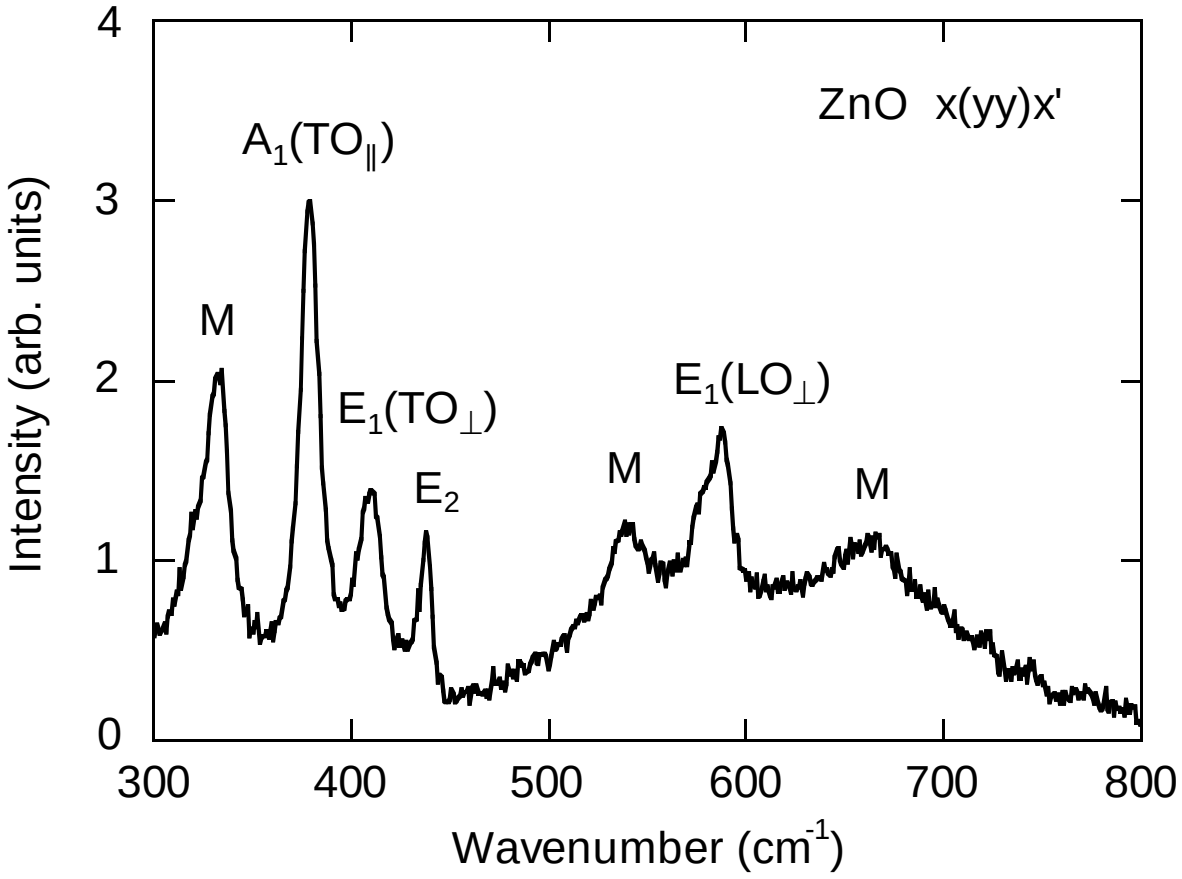
ZnO x(yy)x'
A1(TO∥)
M
E1(TO⊥)
E2
M
E1(LO⊥)
M
Intensity (arb. units)
Wavenumber (cm-1)
0
1
2
3
4
300
400
500
600
700
800

Fig. 6